Mechanical Systems and Signal Processing 196 (2023) 110342

Contents lists available at ScienceDirect

Mechanical Systems and Signal Processing

journal homepage: www.elsevier.com/locate/ymssp

Extreme parametric resonance oscillations of a cantilever: An exact theory and experimental validation

Hamed Farokhi [a,*], Eetu Kohtanen [b], Alper Erturk [b]

[a] Department of Mechanical and Construction Engineering, Northumbria University, Newcastle upon Tyne NE1 8ST, UK
[b] George W. Woodruff School of Mechanical Engineering, Georgia Institute of Technology, Atlanta, 30332, USA

ARTICLE INFO

Keywords:
Parametric resonance
Nonlinear vibrations
Geometrically exact model
Extreme cantilever oscillations
Experimental validation

ABSTRACT

Flexible cantilevered beams are capable of undergoing motions of extremely large amplitudes which are relevant to both conventional and emerging applications. However, modelling and capturing such behaviour is not a straightforward task and requires the application of a geometrically exact model. In this study, the extreme parametric resonance responses of a cantilever with a tip mass are captured through carefully conducted experimental measurements and compared to the predictions of a centreline-rotation-based geometrically exact cantilever beam model. For the experimental part, a state-of-the-art in-vacuo base excitation set-up consisting of a vacuum chamber and a long-stroke shaker is utilised to excite the cantilever in the axial direction near parametric resonance and drive the cantilever to very large oscillation amplitudes. This set-up is accompanied by a high-speed camera to capture footage of the deformed configurations of the cantilever in a period of steady-state oscillations at each excitation frequency. The cantilever motion amplitudes are then extracted from the videos through use of a robust image processing code. For the theoretical modelling and numerical analysis parts of the study, the cantilever is modelled via the Euler–Bernoulli beam theory assuming an inextensible centreline, while considering the centreline rotation as the main motion variable. All nonlinear terms in the model are kept intact throughout the derivation, discretisation, and simulation procedures to ensure accurate model predictions. Comparisons between experimental and theoretical results are conducted for three axial base-acceleration levels. It is shown that the geometrically exact model's predictions are in excellent agreement with experimental results at various oscillation amplitudes.

1. Introduction

Cantilevers are beams with one fixed and one free end, and they are present in many mechanical structures and systems [1–5]. Owing to having one end free, they are well-suited for many applications such as micro gyroscopes, micro/nano-electromechanical systems (MEMS/NEMS), vibration and flow-based energy harvesters, bio-inspired locomotion mechanisms, and different types of piezoelectric and MEMS/NEMS-based sensors [6–15]. Furthermore, due to having one end free, they can be excited to undergo large-amplitude vibrations to the extent that flapping occurs, i.e. with the tip bending backwards, while staying in the elastic regime with a proper choice of material; this behaviour is of particular interest in applications where such large-amplitude vibration is desirable such as inverted flag flow-based energy harvesters [16–18]. Another completely different area of interest for extreme oscillations of cantilevers is computer graphics for simulating hair, grass, and vegetation motions [19,20]. However, developing a model that

* Corresponding author.
E-mail address: hamed.farokhi@northumbria.ac.uk (H. Farokhi).

https://doi.org/10.1016/j.ymssp.2023.110342
Received 22 November 2022; Received in revised form 28 February 2023; Accepted 1 April 2023
Available online 6 April 2023

is capable of capturing such large-amplitude dynamics is not an easy task, since at extreme motion amplitudes, the assumptions of nonlinear truncated models, such as the commonly used third-order nonlinear model, become invalid hence requiring application of so-called geometrically exact models.

Dynamical characteristics of cantilevers have been the topic of investigation by many researchers over the last few decades, with earlier investigations conducted by Crespo da Silva and Glynn [21,22], who developed the equations governing the in-plane and out-of-plane motions of a cantilever by assuming an inextensible centreline and considering nonlinearities up to third order, and solved the equations using the method of multiple scales. These efforts were continued by Nayfeh and Pai [23,24], who investigated the lateral dynamics of base-excited cantilevers using a third-order model and the method of multiple scales. The non-planar nonlinear dynamics of cantilevers under parametric excitation was also studied by Nayfeh and co-investigators [25]. Further investigations were carried out by, for instance, Feng and Leal [26], who focused on the symmetries in cantilevered beam equations with inextensibility assumption, Hsieh et al. [27], who examined relatively large-amplitude vibrations of a cantilever using the nonlinear vibration modes, and Oh and Nayfeh [28], who shed light on the combination resonances in composite plate cantilevers. On the topic of parametric resonance, Carboni et al. [29] proposed a nonlinear Euler–Bernoulli model for slender piezoelectric beams to examine the parametric resonance response due to an in-plane piezoelectric actuation by a pulsating voltage with a DC component; they utilised the method of the multiple scales up to the fifth order to directly solve the partial differential equation of motion.

There have been many other investigations on the free and forced dynamics of cantilevers [30,31]. For instance, Zhang et al. [32] studied the chaotic behaviour of a cantilever under both axial and transverse base excitations utilising the multiple scales method together with the Galerkin discretisation scheme. Yoo et al. [33] conducted an experimental analysis to investigate the relatively large-amplitude vibrations of a cantilever to examine the accuracy of the absolute nodal coordinate formulation method for dynamic analysis of cantilevers. Further investigation was carried out by Dwivedy and Kar [34], who examined the nonlinear dynamics of a base-excited cantilevered beam with a tip mass considering internal resonances. Another theoretical-experimental investigation was conducted by Mahmoodi et al. [35], who examined the nonlinear vibration of cantilevered viscoelastic beams employing the method of multiple scales. A third-order nonlinear cantilever model was used by Thomas et al. [36], who studied the response characteristics of a rotating cantilever beam, focusing on the frequency response diagrams and the softening/hardening nonlinear behaviour of the cantilever. Huang et al. [37] conducted an experimental study on hardening effects in rotating cantilevers; they utilised the digital image correlation and phase mapping method to conduct direct measurements under operational conditions. They obtained full field displacement responses of the cantilevers as well as their natural frequencies and compared the results to those of a finite element model. Utzeri et al. [38] examined the large-amplitude nonlinear vibrations of a composite beam with and without a lumped mass attached along its length; they used both analytical and finite element models to predict the response and compared the theoretical results to experimental observations. Further investigation on this topic was carried out by Touzé and Thomas [39], who utilised the method of nonlinear normal modes [40–42] together with a third-order model to analyse the large-amplitude vibrations of a cantilever using a time integration method, Colin et al. [43], who conducted a theoretical-experimental investigation and proposed a quadratic air damping model for structures undergoing large-amplitude oscillations, and Shen et al. [44], who conducted extensive comparisons of model-order reduction methods for geometrically nonlinear structures. The third-order nonlinear cantilever model has been utilised in several other studies on, for instance, piezoelectric actuators, sensors, and vibration energy harvesters [45–50]. Farokhi et al. [51,52] continued the research on this topic by developing a rotation-based geometrically exact nonlinear cantilever model capable of examining nonlinear oscillations of extremely large amplitudes. This rotation-based exact model was utilised for dynamical analysis of inverted flags as well by Tavallaeinejad et al. [53,54]. In an interesting recent study, Debeurre et al. [55] proposed a finite element-based method for simulation of extreme oscillations of highly flexible slender structures using a geometrically exact two-dimensional beam model; they utilised the harmonic balance method together with the asymptotic numerical method to solve the discretised equations and showcased the capability of their method for different configurations.

Different researchers have developed and utilised geometrically exact models in their research; it should be highlighted that the term "geometrically exact" specifies that the geometric nonlinearities associated with the rotation of the cross section are kept exact (and not truncated) and this is the common characteristic of all geometrically exact models. More details can be found in the book by Géradin and Cardona [56] and the studies by Zupan et al. [57] and Meier et al. [58] for an overview of geometrically exact models in the context of finite-element formulation. In other attempts of large-amplitude cantilever oscillations modelling, Lang et al. [59] proposed a model on the basis of the Cosserat's geometrically exact theory of rods [60] for analysing rods in extension, shear, bending, and torsion. In another study, Bergou et al. [19] developed the method of discrete elastic rods, that was originally proposed for modelling hair motion in computer graphics, considering a different approach for kinematics and dynamics treatment; they verified their model via comparison to experiments. Virgin and Plaut [61] examined the large deflections of a folded cantilever experimentally and theoretically; they conducted an elastica analysis, allowing for large deflections and rotations. Romero et al. [20] proposed a new framework to examine the physical validity of numerical computer graphics simulators for rods, plates, and frictional contact. A note should be made here that these valuable studies solve the spatially discretised equations of motion using direct time integration. In this study, the geometrically exact model of the cantilever is set up in a different way by using the centreline slope as the primary motion variable which relates to longitudinal and transverse displacements through the inextensibility assumption.

To the best knowledge of the authors, there has been no investigation so far to examine the parametric resonance response of a cantilever undergoing extreme oscillations experimentally and compare that against an accurate theoretical model. In a recent experimental-theoretical study by Farokhi et al. [62], the extreme motions of a transversely excited cantilever was examined. The present study focuses on parametric resonance response of an axially excited cantilever with a tip mass which poses several

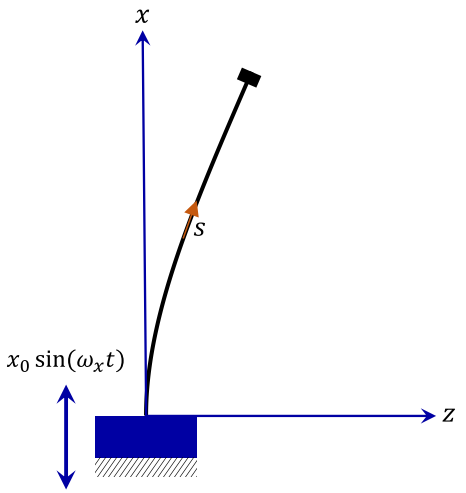

Fig. 1. An axially excited cantilever with a tip mass in a vertical configuration.

new challenges for experimental measurements, theoretical modelling, and numerical simulations. This study presents detailed and carefully conducted experimental results on nonlinear extreme oscillations of an axially excited cantilever using an in-vacuo base excitation set-up together with a high-speed camera. On the theoretical side, a rotation-based geometrically exact model is used to predict the response. Extensive comparisons between experimental and theoretical results are presented at different base acceleration levels showing excellent agreements between the experimental observations and theoretical predictions. A supplementary video file is provided as well showing clear visual comparisons between theoretical and experimental results.

2. Rotation-based geometrically exact model

In this section, the procedure for deriving the geometrically exact model for an axially excited cantilever with a tip mass is explained. To this end, a homogeneous cantilevered beam of length L, cross-sectional area A, second moment of area I, Young's modulus E, mass per unit length m, tip mass M, and material damping coefficient η is considered. The cantilever schematic is illustrated in Fig. 1, showing the $(x;z)$ coordinate system (associated with the undeformed configuration) and the curvilinear coordinate s indicating the distance of an element on the cantilever from the clamped end. The cantilever is under axial base-excitation in the form of $x_0 \sin(\omega_x t)$; additionally, it is in a vertical configuration, with the clamped end being at the bottom and the gravity acting downward (as illustrated in Fig. 1).

As mentioned before, here the centreline rotation is used as the main displacement variable in deriving the cantilevered beam equation of motion and all nonlinear terms are kept intact. The centreline rotation-based geometrically exact model allows capturing extremely large oscillation amplitudes which the transverse displacement-based model is not capable of, as shown in detail in Ref. [62]. Some aspects of the derivation procedure in this section follow the works of Nayfeh and co-investigators (e.g. Ref. [63]), utilising an engineering strain measure together with a stress measure that is a consequence of the constitutive laws (see Ref. [36] for more details).

According to the Euler–Bernoulli beam theory, the centreline inextensibility assumption leads to a direct relationships between the centreline slope, ψ, and the transverse and longitudinal displacements, i.e. w and u, respectively, through equations $\sin\psi(s,t) = \partial_s w(s,t)$ and $\cos\psi(s,t) = 1 + \partial_s u(s,t)$, noting that $\partial_s \equiv \partial/\partial s$. Using these equations, one can write the transverse and longitudinal displacements in terms of the centreline slope as

$$w = \int_0^s \sin\psi(\zeta,t)\mathrm{d}\zeta, \qquad u = -\int_0^s \Big(1 - \cos\psi(\zeta,t)\Big)\mathrm{d}\zeta. \tag{1}$$

Having obtained the transverse and longitudinal displacements in terms of the centreline rotation, one can follow the usual derivation of equation of motion for a cantilever while writing the axial strain in terms of ψ and substituting any instances of w and u in terms of ψ using Eq. (1). More specifically, the only non-zero strain component of the beam can be written as $\epsilon_{xx}(s,t) = -z\partial_s\psi(s,t)$, which leads to the following stress–strain relationship based on the Kelvin–Voigt model

$$\sigma_{xx}(s,t) = -z\Big(E + \eta\partial_t\Big)\partial_s\psi(s,t). \tag{2}$$

The variation of the strain energy and that of the gravitational potential energy of the cantilever can be expressed as

$$\delta\mathcal{V}_S(t) = \int_0^L EI\Big[\partial_s\psi(s,t)\delta\Big(\partial_s\psi(s,t)\Big)\Big]\mathrm{d}s, \tag{3}$$

$$\delta \mathcal{V}_G(t) = \int_0^L \Big(m + M\delta_D(s-L)\Big) g \int_0^s \Big(-\sin\psi(\zeta,t)\delta\psi(\zeta,t)\Big)\mathrm{d}\zeta\,\mathrm{d}s, \tag{4}$$

in which δ stands for the variational operator and δ_D denotes the Dirac Delta function; additionally, as noted before, M stands for the cantilever tip mass. Using an integral identity equation [64] and the Dirac Delta function characteristics, Eq. (4) can be reformulated as

$$\delta \mathcal{V}_G(t) = -\int_0^L \Big[m\Big(L-s\Big) + M\Big] g \sin\psi(s,t)\delta\psi(s,t)\mathrm{d}s. \tag{5}$$

In this study, both Kelvin–Voigt and linear viscous energy dissipation mechanisms are considered, the reason for which is explained in detail later in Section 4. Therefore, the virtual work of the Kelvin–Voigt (KV) and linear viscous (LV) damping mechanisms can be expressed as

$$\begin{aligned}
\delta \mathcal{W}_{KV}(t) &= -\int_0^L \eta I \Big[\partial_t\Big(\partial_s\psi(s,t)\Big)\delta\Big(\partial_s\psi(s,t)\Big)\Big]\mathrm{d}s,\\
\delta \mathcal{W}_{LV}(t) &= -\int_0^L c\Big[\partial_t u(s,t)\delta u(s,t) + \partial_t w(s,t)\delta w(s,t)\Big]\mathrm{d}s\\
&= -\int_0^L c\Big[\int_0^s \Big(\partial_t\psi(\zeta,t)\sin\psi(\zeta,t)\Big)\mathrm{d}\zeta \int_0^s \Big(\sin\psi(\zeta,t)\delta\psi(\zeta,t)\Big)\mathrm{d}\zeta\\
&\qquad + \int_0^s \Big(\partial_t\psi(\zeta,t)\cos\psi(\zeta,t)\Big)\mathrm{d}\zeta \int_0^s \Big(\cos\psi(\zeta,t)\delta\psi(\zeta,t)\Big)\mathrm{d}\zeta\Big]\mathrm{d}s,
\end{aligned} \tag{6}$$

where η and c are the material and linear viscous damping coefficients, respectively, noting that u and w terms in the work of linear viscous damping have been replaced with their ψ representations using Eq. (1).

The kinetic energy of the cantilever consists of transverse and longitudinal motions with respect to the clamped end, the rotational inertia, and the base axial motion; hence, the kinetic energy can be expressed as

$$\begin{aligned}
\mathcal{K}(t) = \frac{1}{2}\int_0^L \rho I\Big(\partial_t\psi(s,t)\Big)^2\mathrm{d}s + \frac{1}{2}\int_0^L \Big(m + M\delta_D(s-L)\Big)\Bigg\{\Big[\int_0^s \Big(\partial_t\psi(\zeta,t)\cos\psi(\zeta,t)\Big)\mathrm{d}\zeta\Big]^2\\
+\Big[x_0\omega_x\cos(\omega_x t) - \int_0^s \Big(\partial_t\psi(\zeta,t)\sin\psi(\zeta,t)\Big)\mathrm{d}\zeta\Big]^2\Bigg\}\mathrm{d}s,
\end{aligned} \tag{7}$$

where ρ denotes the mass density.

Substituting Eqs. (3), (5), (6), and (7) into the extended Hamilton's principle, the rotation-based equation of motion of the cantilever with a tip mass under axial base excitation can be obtained as

$$\begin{aligned}
&\rho I\partial_{tt}\psi - EI\partial_{ss}\psi - \eta I\partial_{tss}\psi - \Big(m(L-s)+M\Big)g\sin\psi\\
&+ c\sin\psi\int_s^L\int_0^\xi \Big(\partial_t\psi(\zeta,t)\sin\psi(\zeta,t)\Big)\mathrm{d}\zeta\mathrm{d}\xi + c\cos\psi\int_s^L\int_0^\xi \Big(\partial_t\psi(\zeta,t)\cos\psi(\zeta,t)\Big)\mathrm{d}\zeta\mathrm{d}\xi\\
&+ \sin\psi\int_s^L \Big(m + M\delta_D(\xi-L)\Big)\Big[x_0\omega_x^2\sin(\omega_x t) + \int_0^\xi \Big(\partial_{tt}\psi(\zeta,t)\sin\psi(\zeta,t) + \Big(\partial_t\psi(\zeta,t)\Big)^2\cos\psi(\zeta,t)\Big)\mathrm{d}\zeta\Big]\mathrm{d}\xi\\
&+ \cos\psi\int_s^L \Big(m + M\delta_D(\xi-L)\Big)\int_0^\xi \Big(\partial_{tt}\psi(\zeta,t)\cos\psi(\zeta,t) - \Big(\partial_t\psi(\zeta,t)\Big)^2\sin\psi(\zeta,t)\Big)\mathrm{d}\zeta\mathrm{d}\xi = 0.
\end{aligned} \tag{8}$$

Next, the following dimensionless quantities are defined

$$\begin{aligned}
&S = \frac{s}{L},\quad \Gamma = \frac{mgL^3}{EI},\quad \gamma = \frac{M}{mL},\quad J_d = \frac{\rho I}{mL^2},\quad \tau = \frac{t}{T_0},\\
&c_d = \frac{cL^4}{EIT_0},\quad \Omega = \omega_x T_0,\quad \eta_d = \frac{\eta}{ET_0},\quad a_x = \frac{x_0\omega_x^2 T_0^2}{L},
\end{aligned} \tag{9}$$

where $T_0 = L^2(m/(EI))^{1/2}$. Using these dimensionless quantities, Eq. (8) can be transformed to the following dimensionless form

$$\begin{aligned}
&J_d\partial_{\tau\tau}\psi - \partial_{SS}\psi - \eta_d\partial_{\tau SS}\psi - \Gamma\Big((1-S)+\gamma\Big)\sin\psi\\
&+ c_d\sin\psi\int_S^1\int_0^\xi \Big(\partial_\tau\psi(\zeta,\tau)\sin\psi(\zeta,\tau)\Big)\mathrm{d}\zeta\mathrm{d}\xi + c_d\cos\psi\int_S^1\int_0^\xi \Big(\partial_\tau\psi(\zeta,\tau)\cos\psi(\zeta,\tau)\Big)\mathrm{d}\zeta\mathrm{d}\xi\\
&+ \sin\psi\int_S^1 \Big(1+\gamma\delta_D(\xi-1)\Big)\Big[a_x\sin(\Omega\tau) + \int_0^\xi \Big(\partial_{\tau\tau}\psi(\zeta,\tau)\sin\psi(\zeta,\tau) + \Big(\partial_\tau\psi(\zeta,\tau)\Big)^2\cos\psi(\zeta,\tau)\Big)\mathrm{d}\zeta\Big]\mathrm{d}\xi\\
&+ \cos\psi\int_S^1 \Big(1+\gamma\delta_D(\xi-1)\Big)\int_0^\xi \Big(\partial_{\tau\tau}\psi(\zeta,\tau)\cos\psi(\zeta,\tau) - \Big(\partial_\tau\psi(\zeta,\tau)\Big)^2\sin\psi(\zeta,\tau)\Big)\mathrm{d}\zeta\mathrm{d}\xi = 0.
\end{aligned} \tag{10}$$

Next, the Galerkin method is utilised to discretise the nonlinear integro-partial differential equation of motion of the cantilever, i.e. Eq. (10), into a set of nonlinear ordinary differential equations (ODEs). To this end, first the rotational variable ψ is defined

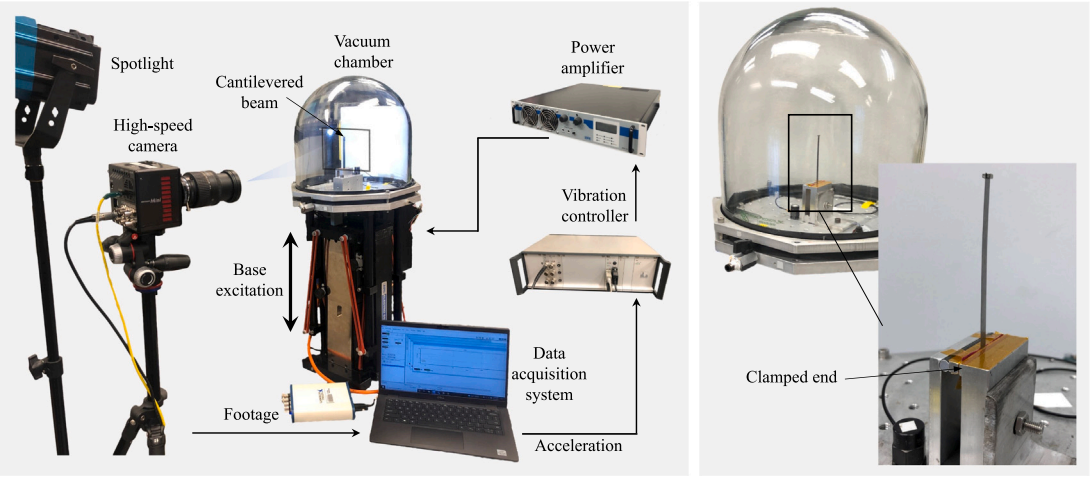

Fig. 2. The experimental set-up used to obtain high-speed video footage of the flexible cantilevered beam at various excitation frequencies in the parametric resonance region.

as a finite series expansion in the form of $\psi(S,\tau)=\sum_{k=1}^{N}\Phi_k(S)q_k(\tau)$, in which $q_k(\tau)$ denotes the kth generalised coordinate for the centreline rotation (which is an unknown time-dependent variable) and $\Phi_k(S)$ stands for its corresponding basis function. $\Phi_k(S)$ is defined as $\partial_S\Delta_k(S)/\beta_k$, where $\Delta_k(S)$ is the kth eigenfunction for the transverse oscillation of a linear cantilever and β_k is the kth root of its transcendental equation. Next, ψ in Eq. (10) is replaced by its series expansion and the Galerkin method is applied, leading to the following set of N nonlinear second-order ODEs

$$
\begin{aligned}
&J_d\sum_{k=1}^{N}\partial_{\tau\tau}q_k(\tau)\left(\int_0^1\Phi_j(S)\Phi_k(S)\mathrm{d}S\right)-\sum_{k=1}^{N}\left(q_k(\tau)+\eta_d\partial_\tau q_k(\tau)\right)\left(\int_0^1\Phi_j(S)\partial_{SS}\Phi_k(S)\mathrm{d}S\right)\\
&-\Gamma\int_0^1\Phi_j(S)\Big((1-S)+\gamma\Big)\sin\left(\sum_{k=1}^{N}\Phi_k(S)q_k(\tau)\right)\mathrm{d}S\\
&+\int_0^1 c_d\Phi_j(S)\left\{\sin\left(\sum_{k=1}^{N}\Phi_k(S)q_k(\tau)\right)\int_S^1\int_0^\xi\left[\left(\sum_{k=1}^{N}\Phi_k(S)\partial_\tau q_k(\tau)\right)\sin\left(\sum_{k=1}^{N}\Phi_k(\zeta)q_k(\tau)\right)\right]\mathrm{d}\zeta\mathrm{d}\xi\right\}\mathrm{d}S\\
&+\int_0^1 c_d\Phi_j(S)\left\{\cos\left(\sum_{k=1}^{N}\Phi_k(S)q_k(\tau)\right)\int_S^1\int_0^\xi\left[\left(\sum_{k=1}^{N}\Phi_k(S)\partial_\tau q_k(\tau)\right)\cos\left(\sum_{k=1}^{N}\Phi_k(\zeta)q_k(\tau)\right)\right]\mathrm{d}\zeta\mathrm{d}\xi\right\}\mathrm{d}S\\
&+\int_0^1\Phi_j(S)\left\{\sin\left(\sum_{k=1}^{N}\Phi_k(S)q_k(\tau)\right)\int_S^1\Big(1+\gamma\delta_D(\xi-1)\Big)\left(\int_0^\xi\left[\left(\sum_{k=1}^{N}\Phi_k(S)\partial_{\tau\tau}q_k(\tau)\right)\sin\left(\sum_{k=1}^{N}\Phi_k(\zeta)q_k(\tau)\right)\right.\right.\right.\\
&\qquad\left.\left.\left.+\left(\sum_{k=1}^{N}\Phi_k(\zeta)\partial_\tau q_k(\tau)\right)^2\cos\left(\sum_{k=1}^{N}\Phi_k(\zeta)q_k(\tau)\right)\right]\mathrm{d}\zeta+a_x\sin(\Omega\tau)\right)\mathrm{d}\xi\right\}\mathrm{d}S\\
&+\int_0^1\Phi_j(S)\left\{\cos\left(\sum_{k=1}^{N}\Phi_k(S)q_k(\tau)\right)\int_S^1\Big(1+\gamma\delta_D(\xi-1)\Big)\int_0^\xi\left[\left(\sum_{k=1}^{N}\Phi_k(\zeta)\partial_{\tau\tau}q_k(\tau)\right)\cos\left(\sum_{k=1}^{N}\Phi_k(\zeta)q_k(\tau)\right)\right.\right.\\
&\qquad\left.\left.-\left(\sum_{k=1}^{N}\Phi_k(\zeta)\partial_\tau q_k(\tau)\right)^2\sin\left(\sum_{k=1}^{N}\Phi_k(\zeta)q_k(\tau)\right)\right]\mathrm{d}\zeta\mathrm{d}\xi\right\}\mathrm{d}S=0,\qquad j=1,2,\ldots,N.
\end{aligned}
\tag{11}
$$

As seen in Eq. (11), all nonlinear terms are kept intact during the discretisation process which makes it significantly challenging since the spatial integrations cannot be performed in closed form and need to be carried out numerically while retaining sufficient terms. This process leads to a very large set of nonlinear ODEs which ensures reliable predictions even at extremely large oscillation amplitudes. In this study, six degrees of freedom are considered by setting $N=6$ which ensures converged results. The discretised model is solved using a pseudo-arclength continuation technique via the AUTO-07P code package [65]. More specifically, the AUTO package is utilised to directly solve the discretised equations of motion and obtain families of stable and unstable periodic solutions; the stability analysis is conducted through computing the Floquet multipliers. It is worth noting that once the rotational time-dependent generalised coordinates are obtained numerically, the transverse and longitudinal displacements are calculated using Eq. (1).

Table 1
Geometric dimensions and material characteristics of the tempered stainless steel beam.

Young's Modulus	E	200 GPa
Density	ρ	7880 kg/m^3
Thickness	h	0.0762 mm
Width	b	4.95 mm
Length	L	72 mm

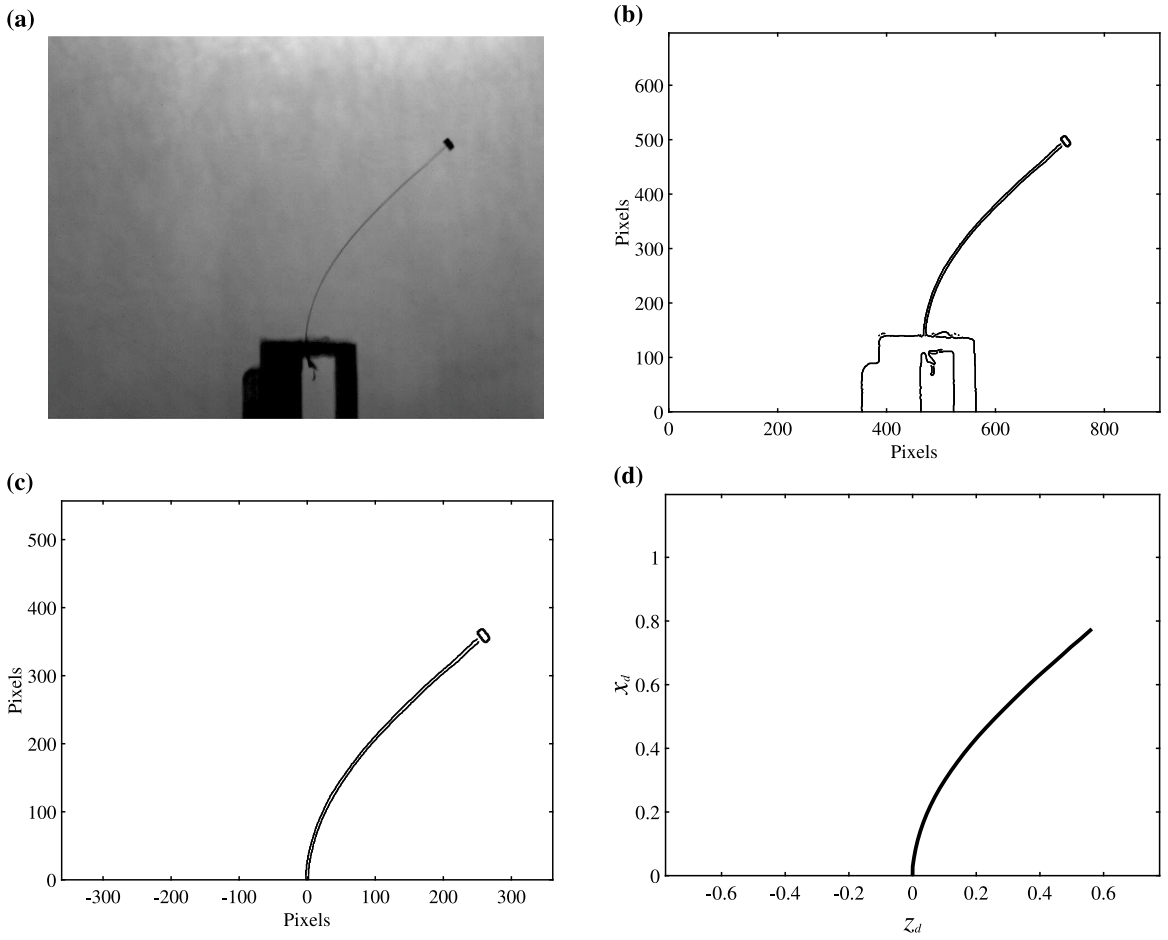

Fig. 3. Different steps of the image processing algorithm: (a) importing one frame of a video footage; (b) detecting the edges of the cantilever and the clamped base in the frame; (c) removing the clamped base edges and resetting the position so that the base is at the coordinate origin; (d) converting the edge profile into a line and dividing the deformed shape by the total length to obtain the dimensionless deformed configuration.

3. Experimental set-up and image processing method

The parametric resonance response of the cantilever is examined experimentally using the set-up shown in Fig. 2. The set-up features a flexible cantilever excited by a long stroke shaker (APS-113) that actuates the base vertically (i.e. in the axial direction of the cantilever). The beam is made of tempered stainless steel and hosts two tip masses symmetric about the centreline and attached with a thin 10-micron layer of epoxy (3M DP-460); the total added tip mass is 0.122 g resulting in an experimentally measured first natural frequency of 6.0 Hz. The tip masses are necessary to reduce the required base acceleration level for driving the cantilever to extreme oscillation amplitudes within the shaker performance envelope. The cantilever is placed inside a vacuum chamber held at 1% atmospheric pressure and mounted onto the shaker armature to further increase the beam oscillation amplitude by minimising air damping effects. The relevant material and geometric properties of the beam are shown in Table 1. The shaker is driven by an APS-125 power amplifier with an input signal from the SPEKTRA VCS-201 vibration controller. The controller uses feedback from the base acceleration signal to maintain a specified RMS acceleration level. The base acceleration is measured with a C114973 Kistler accelerometer mounted next to the beam clamped end.

To ensure steady state oscillations, the controller performs a frequency sweep at the lowest allowable sweep rate (0.05 Hz/min). The sweeps are conducted near twice the beam's fundamental natural frequency and cover excitation frequencies for which the

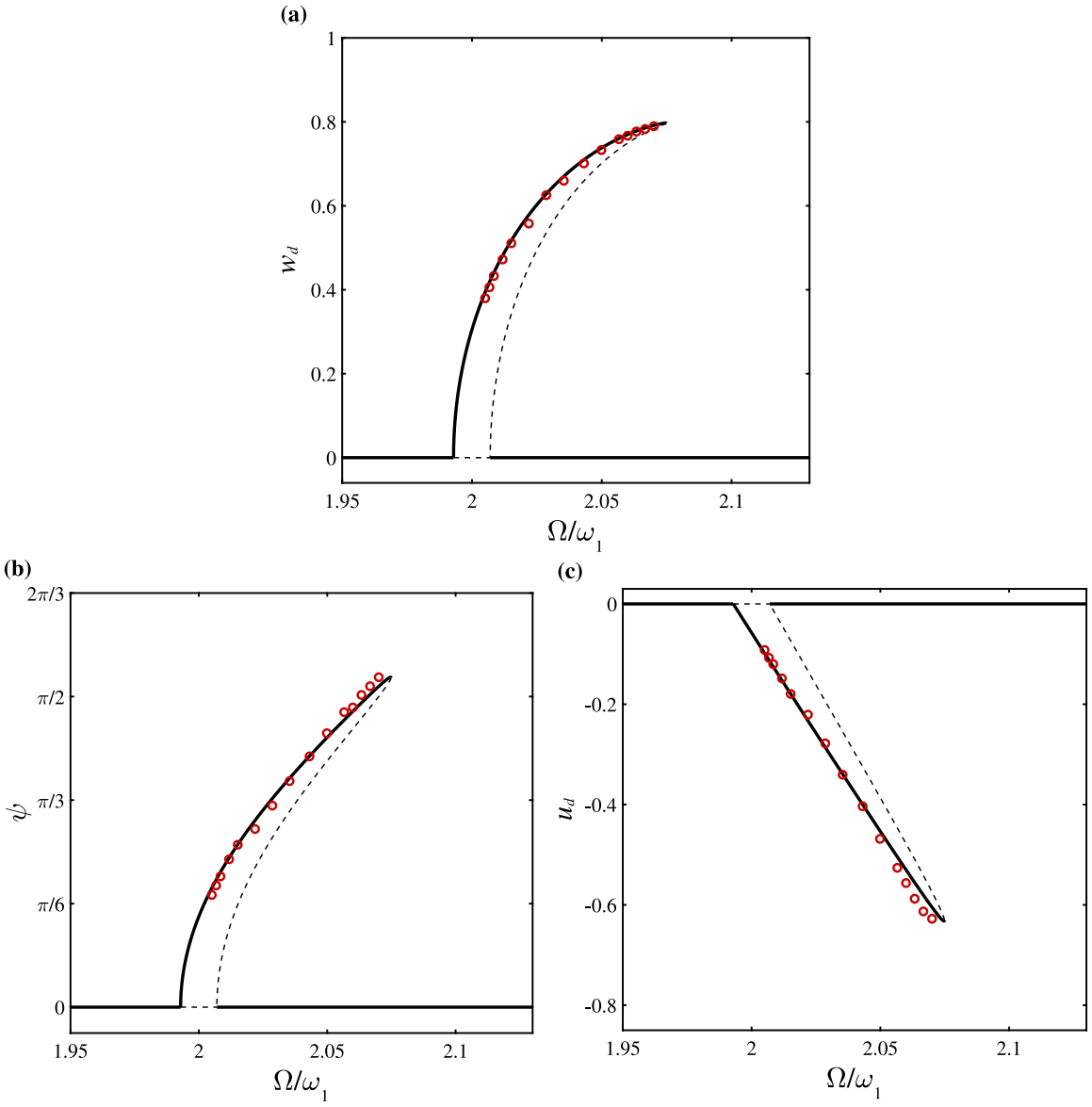

Fig. 4. Parametric resonance response of the cantilevered beam with the tip mass at 0.15 g RMS axial base acceleration level (i.e. $a_x = 0.0632$); (a–c) show the frequency responses of the maximum transverse, rotational, and longitudinal motion amplitudes at the tip of the cantilever, respectively. [o]: experimental results; [——]/[- - -]: stable/unstable solutions based on the exact model.

response of the beam is nonzero. Video footage of the beam vibration is obtained with a high-speed camera (Photron MINI AX200) using a rate of 2000 frames per second at select frequencies that span the sweep range. The number of frames is set to 720 for each video, which covers at least two full vibration cycles. A spotlight is directed at the beam with a white background to enhance contrast for image processing at later stages. Three different RMS acceleration levels are examined, i.e. 0.15 g, 0.20 g, and 0.25 g, with g denoting the gravitational acceleration, and an average of 21 videos are recorded at each excitation level. After obtaining the footage, an image processing method is used to extract the cantilever displacements and rotation magnitudes from each video.

More specifically, the robust image processing code is developed in MATLAB, using an edge detection algorithm,[1] to extract the deformed shape of the cantilever at each frame and the tip displacements and rotation from the deformed shape. Different steps of the image processing algorithm are shown in Fig. 3. More specifically, for each frame of each video footage, first the edges of the cantilever and the clamped base are extracted using an edge detection algorithm. The clamped base edges are then removed and

[1] https://uk.mathworks.com/help/images/ref/edge.html.

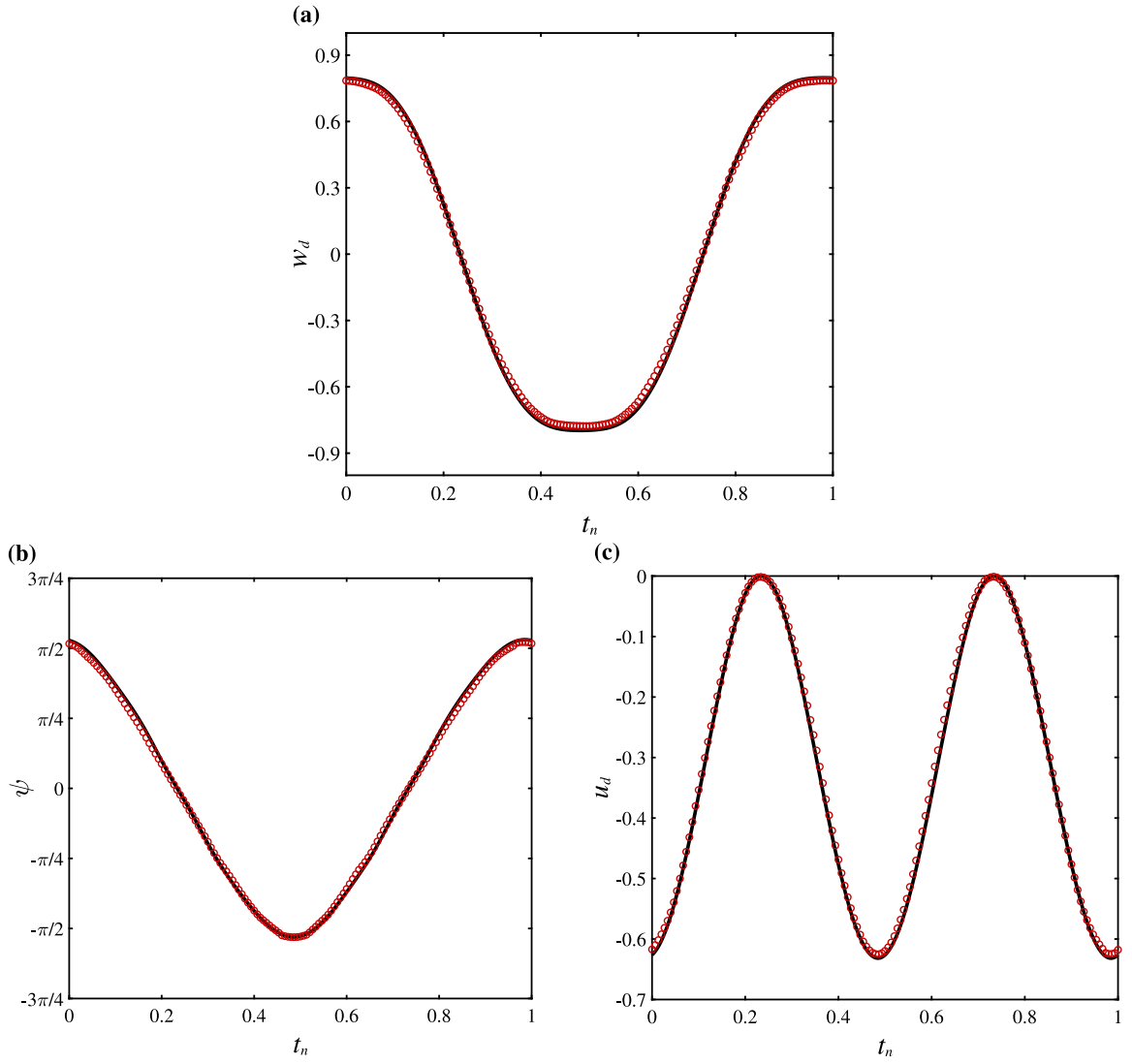

Fig. 5. Time histories of the cantilever peak tip (a) transverse displacement, (b) rotation, and (c) longitudinal displacement, for the system of Fig. 4 in one period of oscillation. t_n denotes normalised time with respect to the period of oscillation. Experimental and theoretical results are shown by [o] and [—], respectively.

the pixels of the cantilever edges are moved such that the base is at the coordinate origin, i.e. $(0, 0)$. Then the edge profile of the cantilever with the tip mass is converted into a solid line and nondimensionalised with respect to its length, allowing for the tip displacements to be extracted. To extract the tip rotation, a linear fitting was used on the points constructing the last 5% of the length of the cantilever (close to the tip) and the slope of that line was obtained, from which the tip rotation was calculated.

4. Detailed theoretical-experimental results and discussions

The parametric resonance response of the cantilever with a tip mass is investigated in this section theoretically and experimentally. More specifically, the theoretical calculations are conducted using the geometrically exact model developed in Section 2 and compared extensively to the experimental observations. It should be noted that all the results in this section are presented in nondimensional form. As mentioned in the previous section, three sets of experiments are conducted at RMS acceleration levels of 0.15 g, 0.20 g, and 0.25 g. In what follows, detailed comparisons are carried out between the theoretical and experimental results at these three base acceleration levels.

An important note should be made about the damping and its implications. As mentioned in Section 2, both linear viscous damping and Kelvin–Voigt damping mechanisms are considered in the cantilever model development. Although the Kelvin–Voigt damping term appears as a linear model with respect to ψ in the equation of motion, it is in fact a nonlinear damping model

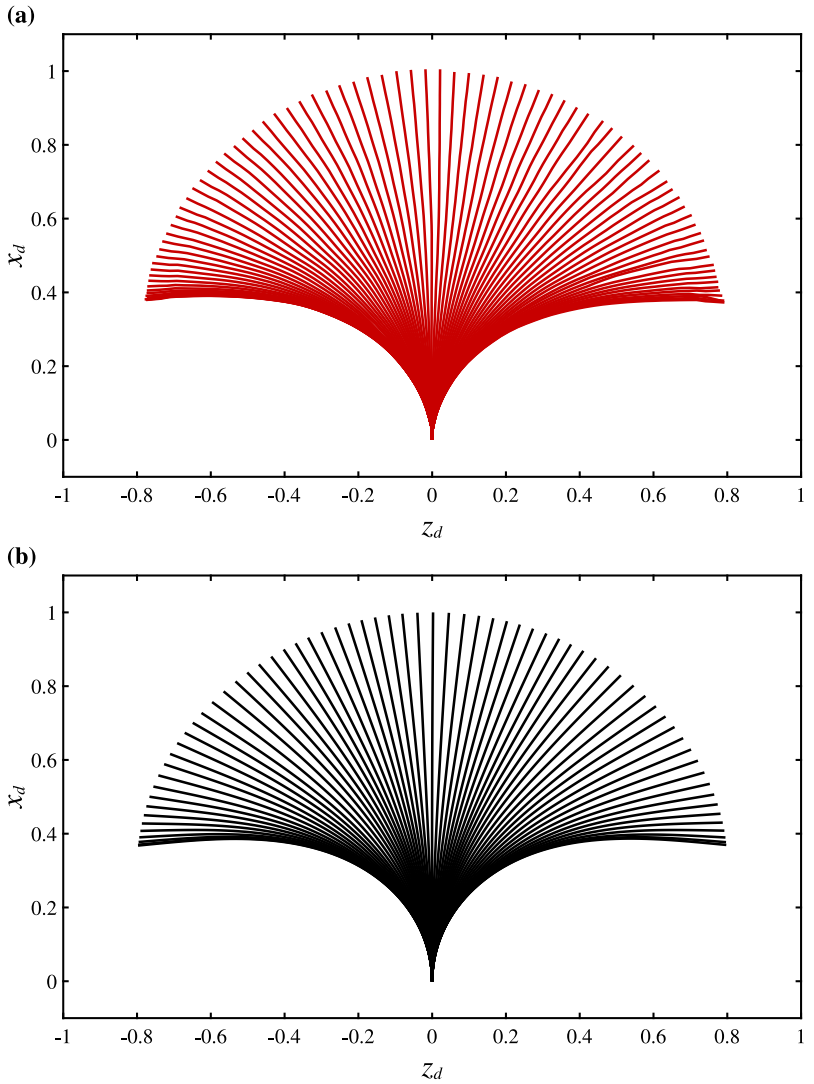

Fig. 6. (a) Experimental and (b) theoretical peak amplitude oscillation of the cantilever of Fig. 4 in one period. For a more detailed comparison, refer to the provided supplementary video file.

with respect to u and w due to the nonlinear relationships between ψ and the longitudinal/transverse displacements. In contrast, the linear viscous damping terms appear as nonlinear terms in the ψ equation of motion, but in fact they have a linear damping effect on u and w motions. The goal here is to propose a robust damping mechanism by keeping the damping coefficients fixed as the base acceleration level is increased. Our investigation showed that considering only Kelvin–Voigt damping with a fixed coefficient calibrated using lowest base acceleration level will underestimate the peak amplitude at higher excitation levels; on the other hand, considering only a linear viscous damping model with a fixed coefficient calibrated using lowest base acceleration level, will overestimate the amplitude at higher levels of excitation. Hence, this issue is resolved by considering both linear viscous damping and Kelvin–Voigt damping mechanisms. Hence, for all the theoretical simulations conducted in this section, the dimensionless linear damping coefficient c_d is set to 0.034 and the dimensionless material damping coefficient η_d is set to 0.0023.

Other dimensionless parameters, which will be kept constant for all simulations, are obtained as $\Gamma = 0.298$, $\gamma = 0.570$, and $J_d = 2.5 \times 10^{-12}$, based on the values given in Table 1 and considering a total added tip mass of 0.122 g. Furthermore, in what follows, w_d and u_d represent the dimensionless transverse and longitudinal displacements (with respect to the length), respectively, while ω_1 denotes the first dimensionless natural frequency of the cantilever with the tip mass, which relates to its dimensional counterpart $\hat{\omega}_1$ through $\omega_1 = \hat{\omega}_1 T_0$.

Starting with the base acceleration of 0.15 g RMS, Fig. 4 shows the frequency responses of the cantilever with the tip mass in the parametric resonance region for (a) tip transverse displacement, (b) tip rotation, and (c) tip longitudinal displacement. For the axially excited cantilever, the parametric resonance occurs when the excitation frequency is close to twice the primary natural frequency

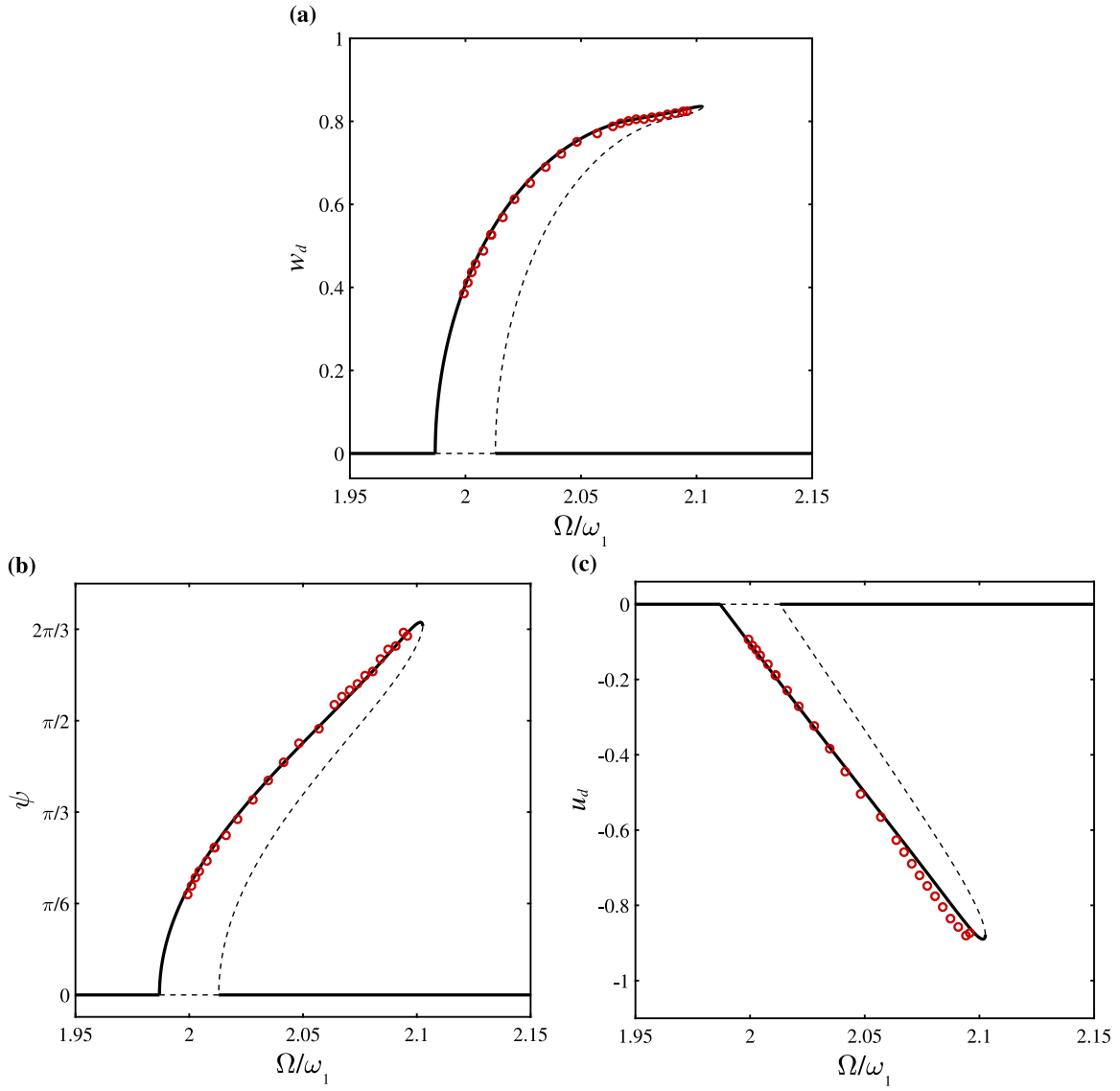

Fig. 7. Parametric resonance response of the cantilevered beam with a tip mass at 0.20 g RMS axial base acceleration level (i.e. $a_x = 0.0843$); (a–c) show the frequency responses of the maximum transverse, rotational, and longitudinal motion amplitudes at the tip of the cantilever, respectively. [o]: experimental results; [—]/[- - -]: stable/unstable solutions based on the exact model.

of the system and the base acceleration is larger than a specific threshold. If these conditions are met, then two period-doubling bifurcations appear in the static zero-amplitude branch, giving rise to periodic solution branches, one stable and one unstable. The two branches coincide at a saddle–node bifurcation near the peak amplitude. For the cantilever in this study, the base acceleration needs to be larger than 0.1233 g RMS (as predicted by the exact model) to ensure presence of dynamical solution branches, hence why the minimum base acceleration case is set 0.15 g RMS.

It is seen in Fig. 4 that the proposed geometrically exact model response predictions are very close to the responses obtained experimentally for the tip transverse and longitudinal displacements as well as the tip rotation. It is worth noting that even for this case, which is the smallest base acceleration examined, the cantilever undergoes very large oscillation amplitudes with the tip transverse displacement reaching around 80% of the length, and the tip slope exceeding $\pi/2$. The presence of a hardening nonlinear behaviour is evident as observed experimentally and predicted by the model. The time histories of the peak cantilever tip motions in one period of oscillation are shown in Fig. 5, again showing the excellent agreement between the experimental observations and the theoretical results. To provide a more visual comparison between the experimental and theoretical results at peak oscillation amplitude, Fig. 6 is constructed showing snapshots of the cantilever motion in one period, further showcasing the accuracy of the proposed model and the precision of the conducted experiments. A supplementary video file is provided which better illustrates the cantilever motion at different excitation levels and the comparison between experimental and theoretical results.

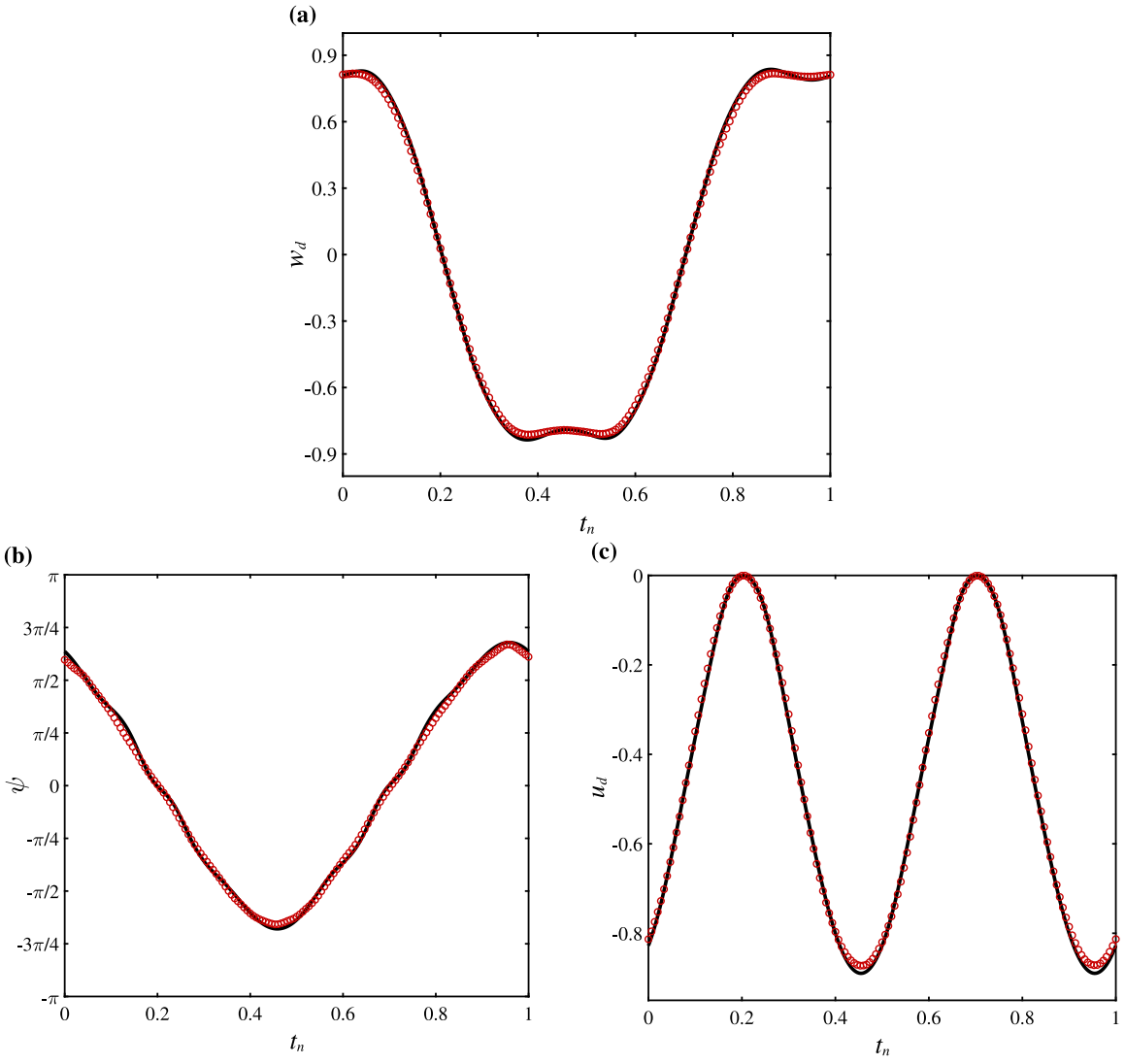

Fig. 8. Time histories of the cantilever peak tip (a) transverse displacement, (b) rotation, and (c) longitudinal displacement, for the system of Fig. 7 in one period of oscillation. t_n denotes normalised time with respect to the period of oscillation. Experimental and theoretical results are shown by [o] and [—], respectively.

Next, the base acceleration is increased to 0.20 g RMS and the parametric resonance frequency responses are constructed both experimentally and theoretically as illustrated in Fig. 7. The damping coefficients are kept at the same values as the previous case. As seen, the geometrically exact model slightly overestimates the peak amplitude, but otherwise the agreement between theoretical and experimental results is very good. Compared to the previous case, it is seen that the maximum tip rotation and longitudinal displacement are clearly increased as a result of increased base acceleration, while the tip transverse displacement peak magnitude does not change much. This is a common behaviour in cantilevers undergoing extreme motions which will be discussed in more detail for the next base acceleration case. To have a closer look at the cantilever response at peak amplitude, the time histories of the tip displacements and rotation are shown in Fig. 8. As seen, the geometrically exact model's predictions are very close to the experimental results. Furthermore, the motion of the cantilever at peak amplitude is illustrated in Fig. 9, showing very similar motion patterns and characteristics between experimental observations and theoretical results. The model predicts that the cantilever displays flapping motion at this base excitation level which is confirmed by the experimental observations. It is worth noting that at this amplitude, the presence of a travelling wave is predicted by the theoretical model; more specifically, looking closely at Fig. 9(b), it is seen that there are two line colours, one being light grey and the other one solid black. The light grey lines show the cantilever motion when it goes from the peak positive transverse amplitude (i.e. fully bent to the right-hand side) to the peak negative transverse amplitude (i.e. fully bent to the left-hand side), while the solid black lines show the motion when it goes from far

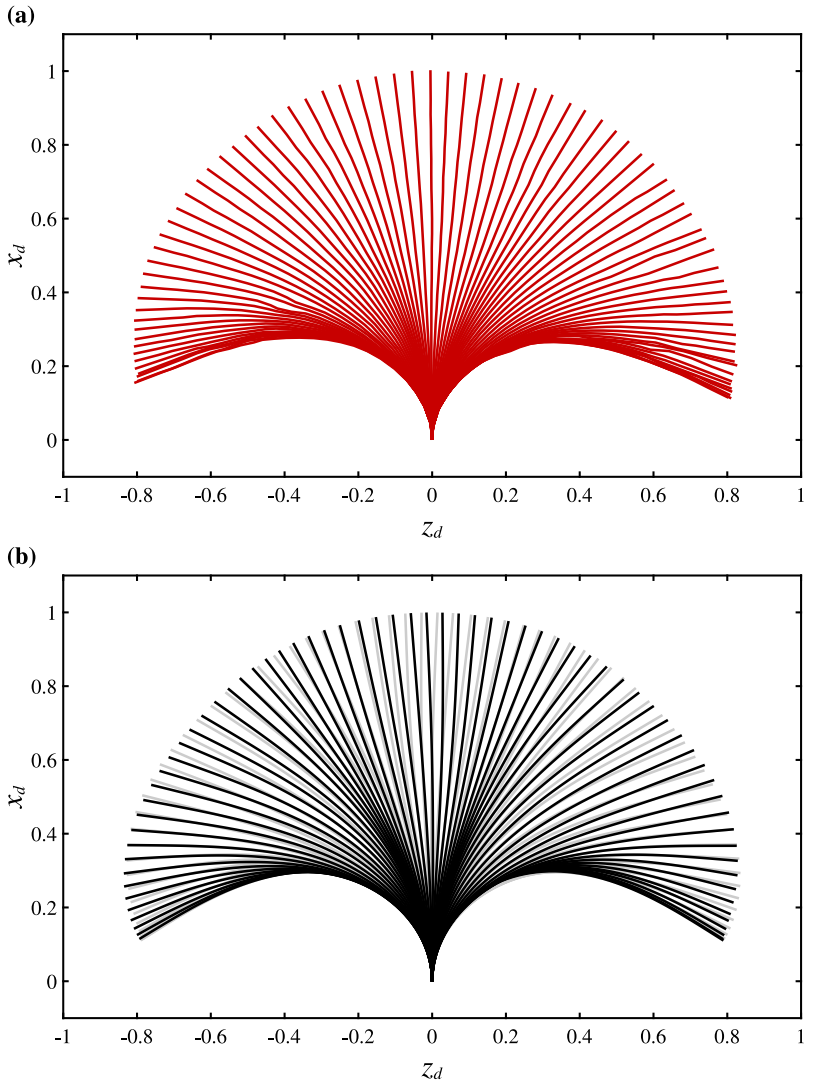

Fig. 9. (a) Experimental and (b) theoretical peak amplitude oscillation of the cantilever of Fig. 7 in one period. For a more detailed comparison, refer to the provided supplementary video file.

left to right. It was difficult to extract this characteristics from the experimental result via image processing, but it can be observed in the original experimental video footage provided in the supplementary video file.

The last experimental-theoretical case examined in this section is for the base acceleration of 0.25 g RMS, and the relevant results are shown in Figs. 10–12. The damping coefficients are kept at the same values as the previous two cases. At this base excitation level, the cantilever displays extremely large oscillation amplitudes with the tip slope reaching almost $3\pi/4$ and the longitudinal displacement exceeding 90% of the length. It is seen in Fig. 10 that even at this extreme level of oscillations, the proposed geometrically exact model provides results that are very close to the experimental observations, showcasing the accuracy and reliability of this model. Compared to the previous case, although both tip rotation and longitudinal displacement magnitudes are clearly increased, the peak magnitude of the transverse displacement is not affected much. This is due to the fact that at this excitation level, the cantilever displays flapping motion in which the tip of the cantilever bends backwards. In such a motion regime, a further increase in the excitation level increases the flapping motion amplitude (i.e. increased tip angle) while not significantly affecting the peak transverse displacement. This behaviour is clearly shown in Fig. 11. Comparing Fig. 11(a) and (b), it is seen that at the time of the maximum tip slope (i.e. when the cantilever reaches either end of the flapping), there is a local minimum in the transverse displacement. In other words, the transverse displacement increases as the tip rotation increases up to a certain level, and then decreases afterwards even though the tip rotation continues increasing. This behaviour can be clearly seen in Fig. 12 for both experimental and theoretical results.

A note should be made here about the longitudinal displacement for the three cases examined and the slight discrepancies between the experimental and theoretical predictions as seen in Figs. 4, 7, and 10, which is more evident for larger base acceleration

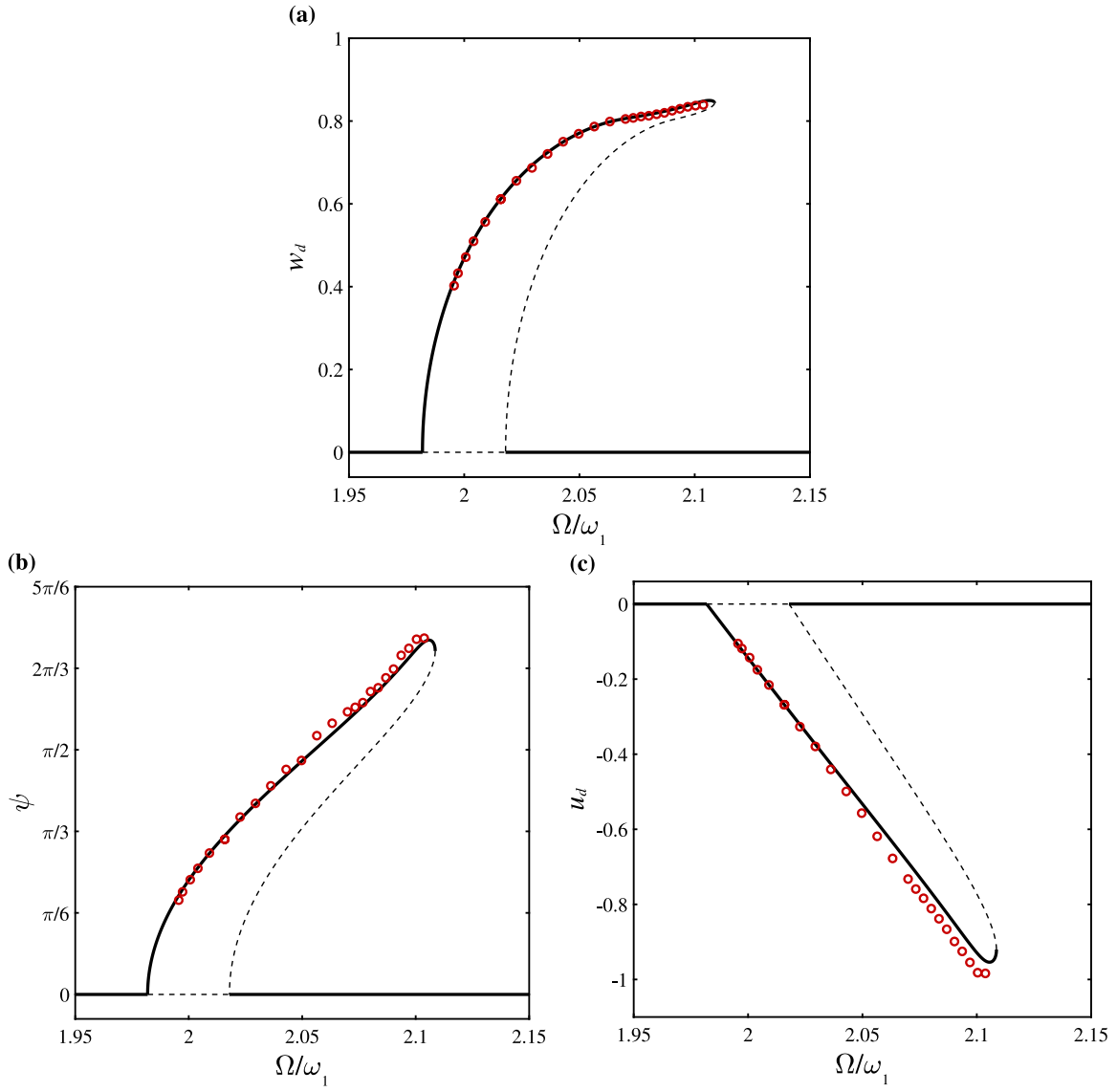

Fig. 10. Parametric resonance response of the cantilevered beam with a tip mass at 0.25 g RMS axial base acceleration level (i.e. $a_x = 0.1054$); (a–c) show the frequency responses of the maximum transverse, rotational, and longitudinal motion amplitudes at the tip of the cantilever, respectively. [o]: experimental results; [▬]/[- - -]: stable/unstable solutions based on the exact model.

cases. The axial displacement magnitude is extracted through measuring the axial location of the end points of the cantilever at both sides of the flapping (i.e. the two extreme sides); however, capturing the cantilever deformed shape via image processing near the two flapping ends has proven to be more difficult. This is exactly the area where there is a slight discrepancy between the experimental and theoretical frequency response curves for the axial displacement. Hence, the authors assume that the slight errors associated with the image processing near the extreme ends could be the reason (at least partly) for this discrepancy. It should be noted that this does not affect the accuracy of the transverse displacement (since the peak occurs before reaching the extreme ends for the case of flapping) or rotation (since it does not depend on the exact location of the end point, but rather the end slope), but it could affect axial displacement since it depends on the exact location of the tip of the cantilever at either side of the flapping.

As mentioned before, a supplementary video file is provided for better visual comparisons between theoretical and experimental results. The video comparisons highlight the high accuracy of the proposed geometrically exact model in capturing extreme motions of the cantilever in the parametric resonance region and the high precision of the conducted experiments. In summary, the theoretical-experimental comparisons shown in this section verify the accuracy of the rotation-based geometrically exact model for examining extreme parametric resonance response of cantilevers.

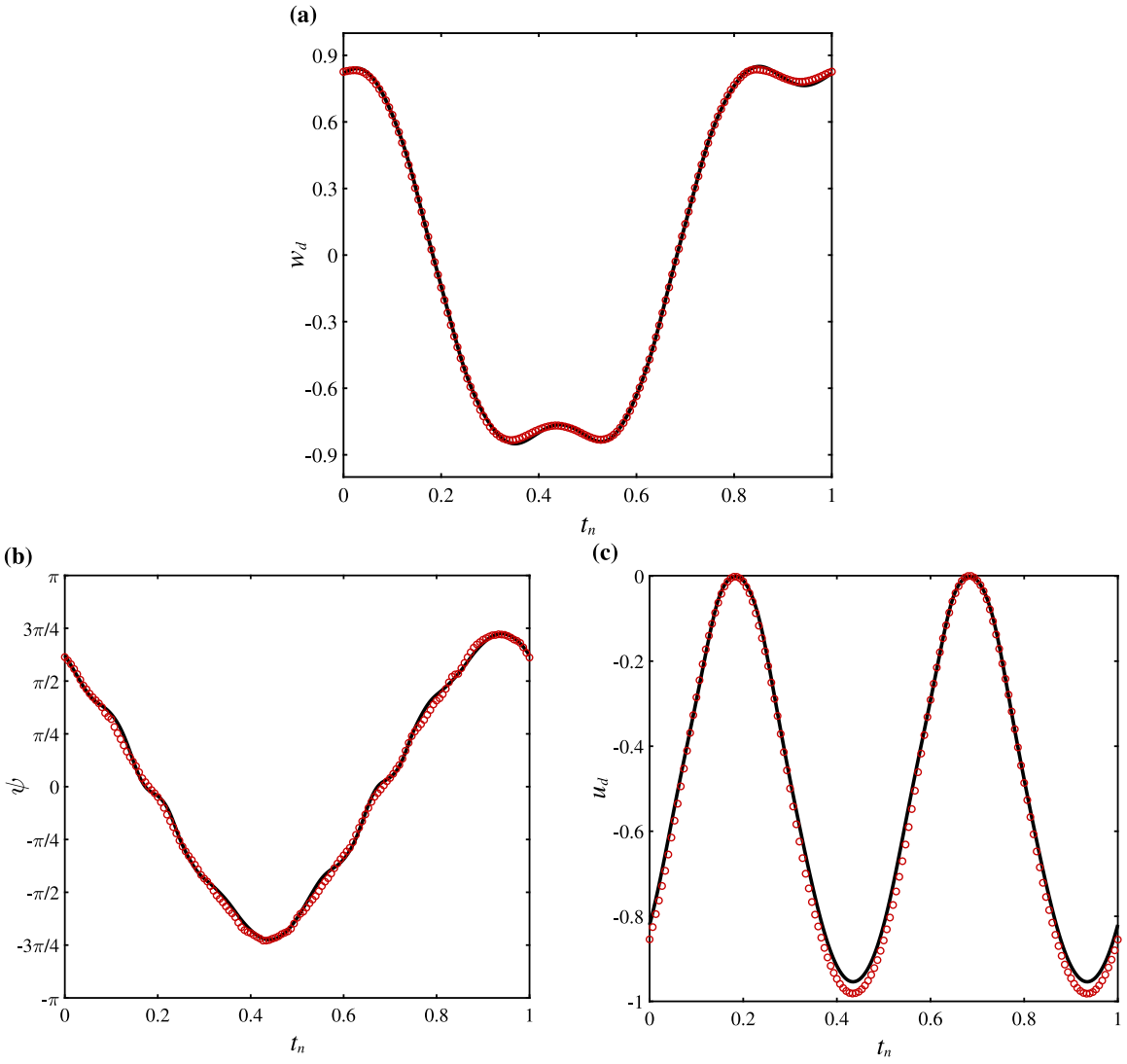

Fig. 11. Time histories of the cantilever peak tip (a) transverse displacement, (b) rotation, and (c) longitudinal displacement, for the system of Fig. 10 in one period of oscillation. t_n denotes normalised time with respect to the period of oscillation. Experimental and theoretical results are shown by [o] and [—], respectively.

5. Further theoretical parametric analysis and discussion

Having verified the accuracy and reliability of the rotation-based exact model, it is utilised in this section to further analyse the effect of different parameters on the response of the cantilever near parametric resonance.

The parametric resonance of the cantilever with the tip mass at various base acceleration magnitudes is examined and illustrated in Fig. 13. A solid red line is drawn connecting the peak magnitudes of the transverse displacement and rotation at each excitation level. It should be noted that this figure includes only theoretical results, and the goal is to provide a quick glance of the evolution of the parametric resonance region with increasing excitation magnitude. All other cantilever parameters are kept the same as the previous cases examined in Section 4. As seen in Fig. 13, for relatively small base acceleration values, there is a sharp increase in the peak transverse displacement and rotation of the cantilever tip as the base acceleration is increased. However, at larger base acceleration levels, the peak transverse displacement reaches almost a plateau and the increase in the peak tip rotation becomes very small.

The effect of gravity is examined in Fig. 14 by constructing the frequency responses of the cantilever for two cases, one taking into account the gravity (i.e. the model used in this study for comparison to experiments), and one neglecting the effect of gravity (i.e. by setting $\Gamma = 0$). It should be noted that the parameter Γ affects the natural frequency. However, in order to better show the effect of this term on the parametric resonance response of the cantilever, the excitation frequency for each case is divided by its

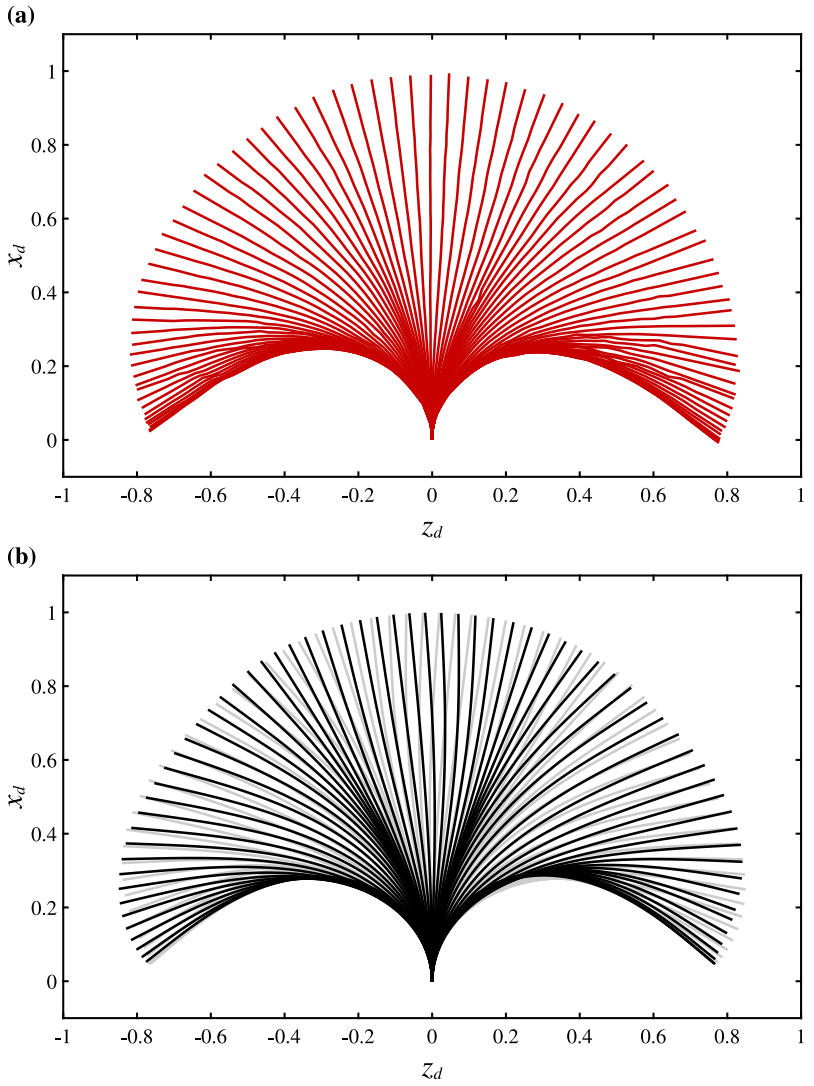

Fig. 12. (a) Experimental and (b) theoretical peak amplitude oscillation of the cantilever of Fig. 10 in one period. For a more detailed comparison, refer to the provided supplementary video file.

corresponding natural frequency (the values of which are provided in the figure caption). As seen, taking into account the effect of gravity clearly strengthens the nonlinear hardening behaviour of the cantilever and increases the peak oscillation magnitude. Additionally, as a result of taking into account the gravitational force, the peak oscillation occurs at a larger excitation frequency ratio compared to the case without gravity. Hence, it is shown that for the vertical configuration of the cantilevered beam with the tip mass examined in this study, the presence of gravity significantly impacts the parametric resonance response and hence must be taken into account in the modelling to ensure reliable predictions.

6. Concluding remarks

A thorough experimental-theoretical investigation was carried out on the extreme parametric resonance response of a cantilever with a tip mass. For the experimental measurements, a thin tempered stainless steel cantilever with a tip mass was placed in a vacuum chamber and the whole set-up was then mounted on a long-stroke axial shaker. The in-vacuo set-up was used to minimise air damping and to be able to drive the cantilever to very large vibration amplitudes. The parametric resonance response of the cantilever was recorded using a high speed camera at three different base acceleration levels. The video recordings were imported into MATLAB in which the deformed shape of the cantilever at each frame was extracted using a robust edge-detection-based image processing code. The experimental frequency responses and time histories were then constructed by extracting the tip displacements and tip rotation from the deformed configuration at each frame. On the theoretical side, a rotation-based geometrically exact model was

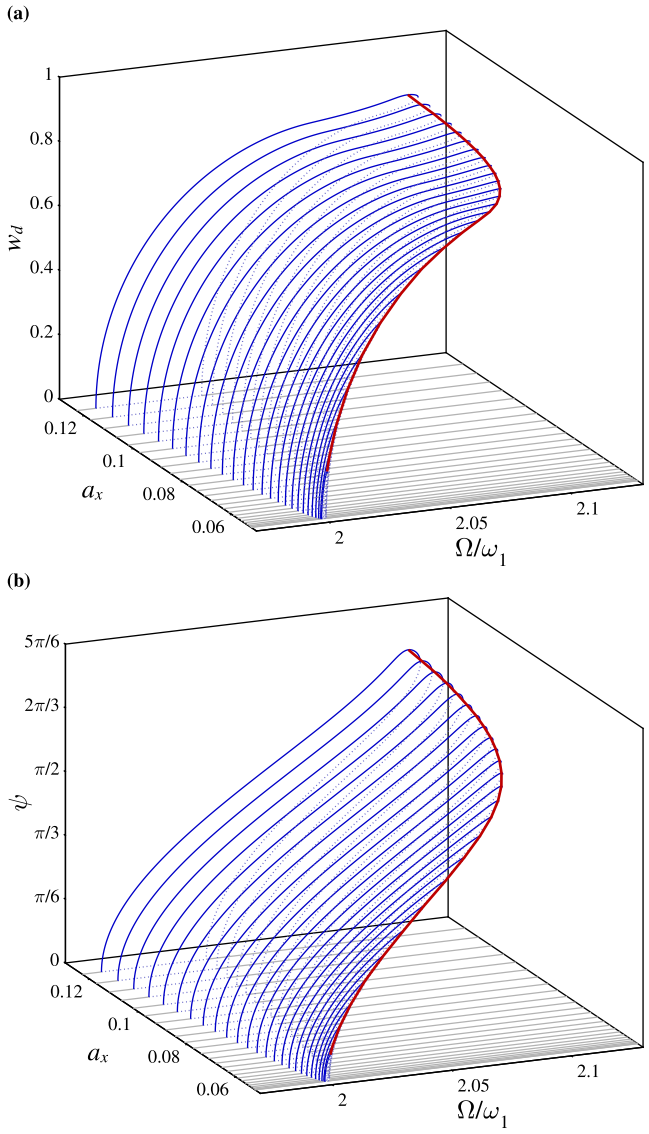

Fig. 13. Frequency responses of the cantilevered beam with the tip mass at various base acceleration levels. Solid and dotted lines show the stable and unstable solutions, respectively.

developed taking into account the effect of tip mass and gravity. A six-degree-of-freedom Galerkin discretisation was implemented and the resultant discretised model was solved using a pseudo-arclength continuation method.

Three sets of experiments were carried out at the axial RMS acceleration levels of 0.15 g, 0.20 g, and 0.25 g. Extensive comparisons were conducted between experimental and theoretical results through frequency response diagrams, time histories, and oscillation snapshots. It was revealed that the cantilever displays a hardening-type nonlinear behaviour in the parametric resonance region. Furthermore, it was shown that even at a relatively small base acceleration (i.e. slightly more than the minimum required to activate parametric resonance), the cantilever undergoes oscillations of very large amplitude, i.e. with a magnitude of around 80% of its length. In order to better assess the robustness of the model in predicting the response amplitudes at various excitation levels without any reparameterisation, the linear viscous and Kelvin–Voigt damping coefficients were kept fixed for all cases. The comparisons revealed that the rotation-based geometrically exact model provides excellent agreement with the experimental results and hence it is fully capable of capturing the parametric resonance response of the cantilever accurately irrespective of the oscillation amplitude.

Finally, having verified the accuracy of the exact model, it was used to examine the parametric resonance response at various excitation levels. It was shown that the oscillation amplitude grows rapidly with increasing base acceleration level at relatively small excitation magnitudes; however, at larger excitation levels, the oscillation magnitude does not change much as the base acceleration

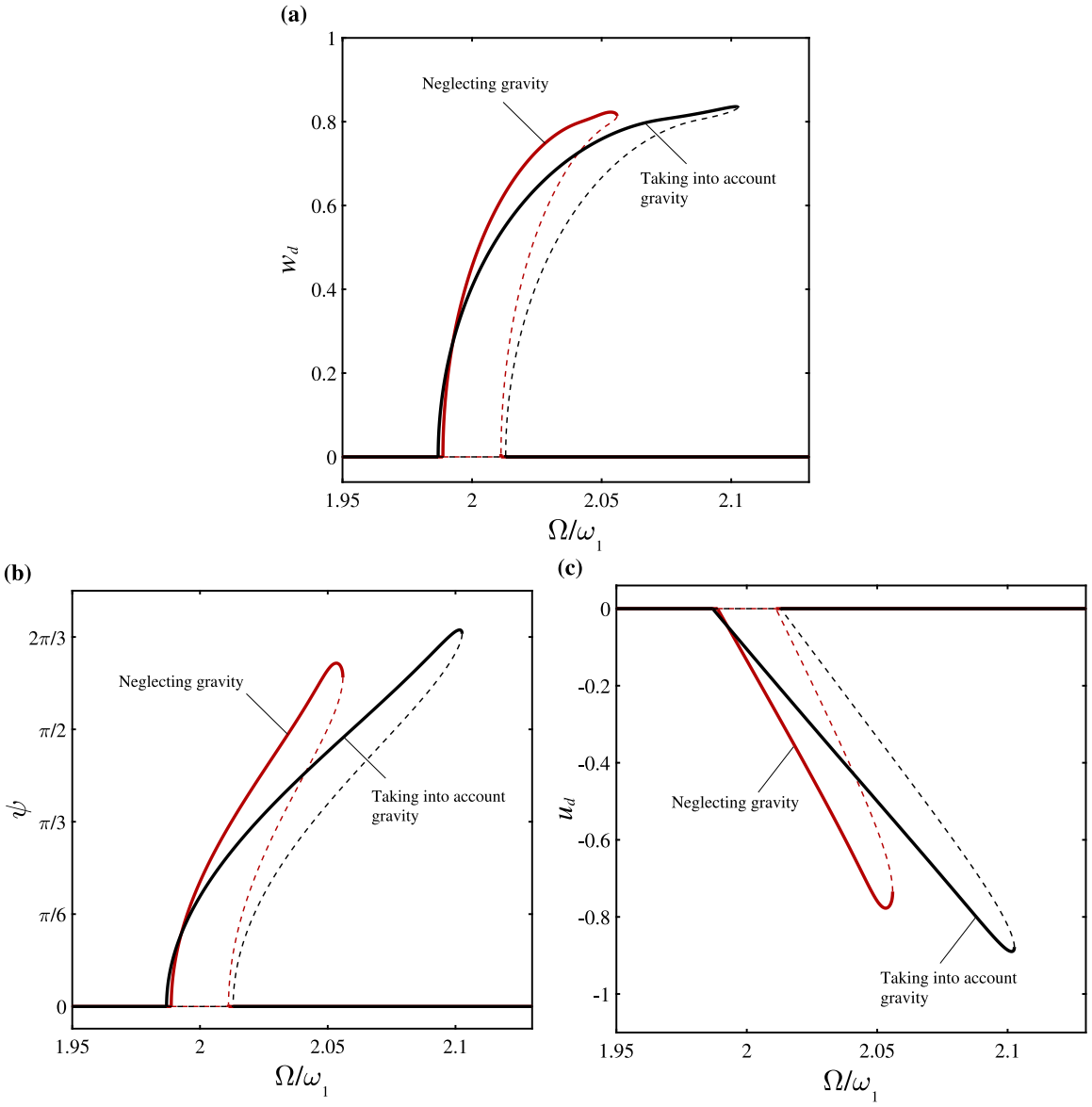

Fig. 14. The effect of gravity on parametric resonance frequency responses of the cantilevered beam with the tip mass at 0.20 g RMS axial base acceleration level (i.e. $a_x = 0.0843$); (a–c) show the frequency responses of the maximum transverse, rotational, and longitudinal motion amplitudes at the tip of the cantilever, respectively. [▬] and [- - -] show the stable and unstable solutions, respectively. $\omega_1 = 1.8250$ for the case with gravity and 1.9288 for the case without gravity.

is increased. Additionally, it was shown that for the configuration examined in this study, gravity significantly affects the parametric resonance response. More specifically, it was shown that when gravity is considered, the cantilever displays a stronger nonlinear hardening behaviour in the parametric resonance response, due to the added axial compressive load from the mass of the cantilever and the tip mass. Hence, it was concluded that for a cantilever in a vertical configuration (with the clamped end at the bottom), the effect of gravity must be accounted for in the modelling to ensure reliable predictions.

CRediT authorship contribution statement

Hamed Farokhi: Conceptualization, Methodology, Formal analysis, Software, Visualization, Validation, Writing – original draft, Writing – review and editing. **Eetu Kohtanen:** Conceptualization, Investigation, Resources, Visualization, Validation, Writing – original draft, Writing – review and editing. **Alper Erturk:** Conceptualization, Investigation, Resources, Writing – review and editing.

Declaration of competing interest

The authors declare that they have no known competing financial interests or personal relationships that could have appeared to influence the work reported in this paper.

Data availability

The datasets generated during and/or analysed during the current study are available from the corresponding author on reasonable request.

A supplementary video file is provided showing detailed video comparisons of the experimental and theoretical results for all cases.

Code availability

The open-source numerical code package utilised in this study for conducting the simulations can be downloaded from https://github.com/auto-07p/auto-07p. More information can be found in Ref. [65].

Appendix A. Supplementary data

Supplementary material related to this article can be found online at https://doi.org/10.1016/j.ymssp.2023.110342.

References

[1] G. Zhang, W. Li, X. Wang, Z. Yang, Influence of flexible structure vibration on the excitation forces delivered by multiple electrodynamic shakers, Mech. Syst. Signal Process. 169 (2022) 108753.
[2] F.M. Foong, C.K. Thein, D. Yurchenko, Structural optimisation through material selections for multi-cantilevered vibration electromagnetic energy harvesters, Mech. Syst. Signal Process. 162 (2022) 108044.
[3] P.V. Katariya, K. Mehar, S.K. Panda, Nonlinear dynamic responses of layered skew sandwich composite structure and experimental validation, Int. J. Non-Linear Mech. 125 (2020) 103527.
[4] Z. Yuan, W. Liu, S. Zhang, Q. Zhu, G. Hu, Bandwidth broadening through stiffness merging using the nonlinear cantilever generator, Mech. Syst. Signal Process. 132 (2019) 1–17.
[5] C.K. Hirwani, S.K. Panda, Numerical nonlinear frequency analysis of pre-damaged curved layered composite structure using higher-order finite element method, Int. J. Non-Linear Mech. 102 (2018) 14–24.
[6] D. Zou, G. Liu, Z. Rao, T. Tan, W. Zhang, W.-H. Liao, Design of vibration energy harvesters with customized nonlinear forces, Mech. Syst. Signal Process. 153 (2021) 107526.
[7] C. Lan, Z. Chen, G. Hu, Y. Liao, W. Qin, Achieve frequency-self-tracking energy harvesting using a passively adaptive cantilever beam, Mech. Syst. Signal Process. 156 (2021) 107672.
[8] J.F. Rhoads, S.W. Shaw, K.L. Turner, Nonlinear dynamics and its applications in micro- and nanoresonators, J. Dyn. Syst. Meas. Control 132 (3) (2010) 034001.
[9] K. Zhou, H. Dai, L. Wang, Q. Ni, P. Hagedorn, Modeling and nonlinear dynamics of cantilevered pipe with tapered free end concurrently subjected to axial internal and external flows, Mech. Syst. Signal Process. 169 (2022) 108794.
[10] A. Shaw, G. Gatti, P. Gonçalves, B. Tang, M. Brennan, Design and test of an adjustable quasi-zero stiffness device and its use to suspend masses on a multi-modal structure, Mech. Syst. Signal Process. 152 (2021) 107354.
[11] C. Zhao, G. Hu, Y. Yang, A cantilever-type vibro-impact triboelectric energy harvester for wind energy harvesting, Mech. Syst. Signal Process. 177 (2022) 109185.
[12] T.D. Caliskan, D.A. Bruce, M.F. Daqaq, Micro-cantilever sensors for monitoring carbon monoxide concentration in fuel cells, J. Micromech. Microeng. 30 (4) (2020) 045005.
[13] W. Wang, J. Cao, C.R. Bowen, Y. Zhang, J. Lin, Nonlinear dynamics and performance enhancement of asymmetric potential bistable energy harvesters, Nonlinear Dynam. 94 (2) (2018) 1183–1194.
[14] S. Jabbari Behrouz, O. Rahmani, S.A. Hosseini, On nonlinear forced vibration of nano cantilever-based biosensor via couple stress theory, Mech. Syst. Signal Process. 128 (2019) 19–36.
[15] F.M. Foong, C.K. Thein, D. Yurchenko, On mechanical damping of cantilever beam-based electromagnetic resonators, Mech. Syst. Signal Process. 119 (2019) 120–137.
[16] U. Latif, E. Uddin, M. Younis, J. Aslam, Z. Ali, M. Sajid, A. Abdelkefi, Experimental electro-hydrodynamic investigation of flag-based energy harvesting in the wake of inverted C-shape cylinder, Energy 215 (2021) 119195.
[17] S. Mazharmanesh, J. Young, F.-B. Tian, J.C. Lai, Energy harvesting of two inverted piezoelectric flags in tandem, side-by-side and staggered arrangements, Int. J. Heat Fluid Flow 83 (2020) 108589.
[18] O. Ojo, Y.-C. Wang, A. Erturk, K. Shoele, Aspect ratio-dependent hysteresis response of a heavy inverted flag, J. Fluid Mech. 942 (2022).
[19] M. Bergou, M. Wardetzky, S. Robinson, B. Audoly, E. Grinspun, Discrete elastic rods, in: ACM SIGGRAPH 2008 Papers, 2008, pp. 1–12.
[20] V. Romero, M. Ly, A.-H. Rasheed, R. Charrondière, A. Lazarus, S. Neukirch, F. Bertails-Descoubes, Physical validation of simulators in Computer Graphics: A new framework dedicated to slender elastic structures and frictional contact, ACM Trans. Graph. (2021).
[21] M. Crespo da Silva, C. Glynn, Nonlinear flexural-flexural-torsional dynamics of inextensional beams. I. Equations of motion, J. Struct. Mech. 6 (4) (1978) 437–448.
[22] M. Crespo da Silva, C. Glynn, Nonlinear flexural-flexural-torsional dynamics of inextensional beams. II. Forced motions, J. Struct. Mech. 6 (4) (1978) 449–461.
[23] A.H. Nayfeh, P.F. Pai, Non-linear non-planar parametric responses of an inextensional beam, Int. J. Non-Linear Mech. 24 (2) (1989) 139–158.
[24] P.F. Pai, A.H. Nayfeh, Non-linear non-planar oscillations of a cantilever beam under lateral base excitations, Int. J. Non-Linear Mech. 25 (5) (1990) 455–474.
[25] H.N. Arafat, A.H. Nayfeh, C.-M. Chin, Nonlinear nonplanar dynamics of parametrically excited cantilever beams, Nonlinear Dynam. 15 (1) (1998) 31–61.

[26] Z. Feng, L. Leal, Symmetries of the amplitude equations of an inextensional beam with internal resonance, J. Appl. Mech. 62 (1) (1995) 235–238.
[27] S.-R. Hsieh, S.W. Shaw, C. Pierre, Normal modes for large amplitude vibration of a cantilever beam, Int. J. Solids Struct. 31 (14) (1994) 1981–2014.
[28] K. Oh, A.H. Nayfeh, Nonlinear combination resonances in cantilever composite plates, Nonlinear Dynam. 11 (2) (1996) 143–169.
[29] B. Carboni, S. Catarci, W. Lacarbonara, Parametric resonances of nonlinear piezoelectric beams exploiting in-plane actuation, Mech. Syst. Signal Process. 163 (2022) 108119.
[30] V. Ondra, B. Titurus, Free vibration and stability analysis of a cantilever beam axially loaded by an intermittently attached tendon, Mech. Syst. Signal Process. 158 (2021) 107739.
[31] L.N. Virgin, D.B. Holland, Experiments on the symmetry-breaking effect of orientation on a pair of connected cantilevers, Mech. Syst. Signal Process. 164 (2022) 108236.
[32] W. Zhang, F. Wang, M. Yao, Global bifurcations and chaotic dynamics in nonlinear nonplanar oscillations of a parametrically excited cantilever beam, Nonlinear Dynam. 40 (3) (2005) 251–279.
[33] W.-S. Yoo, J.-H. Lee, S.-J. Park, J.-H. Sohn, O. Dmitrochenko, D. Pogorelov, Large oscillations of a thin cantilever beam: physical experiments and simulation using the absolute nodal coordinate formulation, Nonlinear Dynam. 34 (1) (2003) 3–29.
[34] S. Dwivedy, R. Kar, Nonlinear dynamics of a cantilever beam carrying an attached mass with 1: 3: 9 internal resonances, Nonlinear Dynam. 31 (1) (2003) 49–72.
[35] S.N. Mahmoodi, N. Jalili, S.E. Khadem, An experimental investigation of nonlinear vibration and frequency response analysis of cantilever viscoelastic beams, J. Sound Vib. 311 (3) (2008) 1409–1419.
[36] O. Thomas, A. Sénéchal, J.-F. Deü, Hardening/softening behavior and reduced order modeling of nonlinear vibrations of rotating cantilever beams, Nonlinear Dynam. 86 (2) (2016) 1293–1318.
[37] J. Huang, K. Wang, J. Tang, J. Xu, H. Song, An experimental study of the centrifugal hardening effect on rotating cantilever beams, Mech. Syst. Signal Process. 165 (2022) 108291.
[38] M. Utzeri, M. Sasso, G. Chiappini, S. Lenci, Nonlinear vibrations of a composite beam in large displacements: analytical, numerical, and experimental approaches, J. Comput. Nonlinear Dyn. 16 (2) (2021).
[39] C. Touzé, O. Thomas, Reduced-order modeling for a cantilever beam subjected to harmonic forcing, in: Proc. of EUROMECH Colloquium, Vol. 457, 2004, pp. 165–168.
[40] C. Touzé, M. Amabili, Nonlinear normal modes for damped geometrically nonlinear systems: Application to reduced-order modelling of harmonically forced structures, J. Sound Vib. 298 (4–5) (2006) 958–981.
[41] C. Touzé, O. Thomas, A. Chaigne, Hardening/softening behaviour in non-linear oscillations of structural systems using non-linear normal modes, J. Sound Vib. 273 (1–2) (2004) 77–101.
[42] C. Touzé, O. Thomas, A. Huberdeau, Asymptotic non-linear normal modes for large-amplitude vibrations of continuous structures, Comput. Struct. 82 (31–32) (2004) 2671–2682.
[43] M. Colin, O. Thomas, S. Grondel, É. Cattan, Very large amplitude vibrations of flexible structures: Experimental identification and validation of a quadratic drag damping model, J. Fluids Struct. 97 (2020) 103056.
[44] Y. Shen, A. Vizzaccaro, N. Kesmia, T. Yu, L. Salles, O. Thomas, C. Touzé, Comparison of reduction methods for finite element geometrically nonlinear beam structures, Vibration 4 (1) (2021) 175–204.
[45] M.I. Friswell, S.F. Ali, O. Bilgen, S. Adhikari, A.W. Lees, G. Litak, Non-linear piezoelectric vibration energy harvesting from a vertical cantilever beam with tip mass, J. Intell. Mater. Syst. Struct. 23 (13) (2012) 1505–1521.
[46] H. Liu, C. Lee, T. Kobayashi, C.J. Tay, C. Quan, Piezoelectric MEMS-based wideband energy harvesting systems using a frequency-up-conversion cantilever stopper, Sensors Actuators A 186 (2012) 242–248.
[47] M. Panyam, M.F. Daqaq, Characterizing the effective bandwidth of tri-stable energy harvesters, J. Sound Vib. 386 (2017) 336–358.
[48] M. Lallart, S. Zhou, Z. Yang, L. Yan, K. Li, Y. Chen, Coupling mechanical and electrical nonlinearities: The effect of synchronized discharging on tristable energy harvesters, Appl. Energy 266 (2020) 114516.
[49] D. Tan, P. Yavarow, A. Erturk, Nonlinear elastodynamics of piezoelectric macro-fiber composites with interdigitated electrodes for resonant actuation, Compos. Struct. 187 (2018) 137–143.
[50] D. Tan, P. Yavarow, A. Erturk, Resonant nonlinearities of piezoelectric macro-fiber composite cantilevers with interdigitated electrodes in energy harvesting, Nonlinear Dynam. 92 (4) (2018) 1935–1945.
[51] H. Farokhi, M.H. Ghayesh, Extremely large oscillations of cantilevers subject to motion constraints, J. Appl. Mech. 86 (3) (2019) 031001.
[52] H. Farokhi, M.H. Ghayesh, Geometrically exact extreme vibrations of cantilevers, Int. J. Mech. Sci. 168 (2020) 105051.
[53] M. Tavallaeinejad, M. Legrand, M.P. Paidoussis, Nonlinear dynamics of slender inverted flags in uniform steady flows, J. Sound Vib. 467 (2020) 115048.
[54] M. Tavallaeinejad, M.P. Païdoussis, M. Legrand, M. Kheiri, Instability and the post-critical behaviour of two-dimensional inverted flags in axial flow, J. Fluid Mech. 890 (2020).
[55] M. Debeurre, A. Grolet, B. Cochelin, O. Thomas, Finite element computation of nonlinear modes and frequency response of geometrically exact beam structures, J. Sound Vib. 548 (2023) 117534.
[56] M. Géradin, A. Cardona, Flexible Multibody Dynamics: A Finite Element Approach, Wiley, 2001.
[57] E. Zupan, M. Saje, D. Zupan, Dynamics of spatial beams in quaternion description based on the Newmark integration scheme, Comput. Mech. 51 (1) (2013) 47–64.
[58] C. Meier, A. Popp, W.A. Wall, Geometrically exact finite element formulations for slender beams: Kirchhoff–Love theory versus Simo–Reissner theory, Arch. Comput. Methods Eng. 26 (1) (2019) 163–243.
[59] H. Lang, J. Linn, M. Arnold, Multi-body dynamics simulation of geometrically exact Cosserat rods, Multibody Syst. Dyn. 25 (3) (2011) 285–312.
[60] S. Antman, Dynamical problems for geometrically exact theories of nonlinearly viscoelastic rods, in: Mechanics: From Theory to Computation, Springer, 2000, pp. 1–18.
[61] L. Virgin, R. Plaut, Large deflections of folded cantilever: Experiments and elastica analysis, Int. J. Non-Linear Mech. 129 (2021) 103641.
[62] H. Farokhi, Y. Xia, A. Erturk, Experimentally validated geometrically exact model for extreme nonlinear motions of cantilevers, Nonlinear Dynam. 107 (1) (2022) 457–475.
[63] A.H. Nayfeh, P.F. Pai, Linear and Nonlinear Structural Mechanics, John Wiley & Sons, 2008.
[64] C. Semler, G. Li, M. Païdoussis, The non-linear equations of motion of pipes conveying fluid, J. Sound Vib. 169 (5) (1994) 577–599.
[65] E.J. Doedel, A.R. Champneys, F. Dercole, T.F. Fairgrieve, Y.A. Kuznetsov, B. Oldeman, R. Paffenroth, B. Sandstede, X. Wang, C. Zhang, AUTO-07p: Continuation and bifurcation software for ordinary differential equations, 2007.